ELSEVIER

International Journal of Mass Spectrometry 192 (1999) 245–257

International Journal of Mass Spectrometry

Electronic versus vibrational excitation in He^{q+} collisions with fullerenes

T. Schlathölter[a,*], O. Hadjar[a], J. Manske[b], R. Hoekstra[a], R. Morgenstern[a]

[a]*KVI Atomic Physics, Rijksuniversiteit Groningen, Zernikelaan 25, 9747AA Groningen, The Netherlands*
[b]*Universität Osnabrück, FB Physik, 49069 Osnabrück, Germany*

Received 23 December 1998; accepted 31 May 1999

Abstract

Collisions of He^{q+} ions with neutral fullerenes have been studied as a function of projectile velocity ($v \approx 0.1$–1.0 a.u.) and charge state ($q = 1, 2$). With increasing velocity, two trends are observed for both charge states: The yield of C_{60-2m}^{r+} clusters decreases with $1/v$, as expected for quantities related to direct vibrational excitation. The relative cross section for multifragmentation increases linearly with v and can be associated with electronic excitations. The additional potential energy of He^{2+} with respect to He^{+} manifests in increased direct ionization cross sections (high v) and multifragmentation cross sections (low v), respectively, revealing information about coupling times between electronic and vibrational excitation. (Int J Mass Spectrom 192 (1999) 245–257) © 1999 Elsevier Science B.V.

Keywords: Fullerenes; Fragmentation; Highly charged ions; Stopping power

1. Introduction

Energy can be deposited into a fullerene by a variety of methods such as electron impact [1], multiphoton absorption [2], or collisions with ions or atoms [3]. In most cases, it is unclear how the resulting excitation couples with the various fragmentation and ionization channels. An open question, in particular, is whether a given excitation mechanism leads to a unique fragmentation pattern. In other words, is it possible to identify excitation processes from their fingerprints in the fragmentation spectra?

Fragmentation patterns from ion–fullerene collisions have been recently studied for a variety of collision systems and energies as well as projectile charge states. Collision energies of less than 250 eV mainly lead to vibrational excitation and bimodal fragment distributions [4]. Similar patterns are also found in photofragmentation studies [2]. This agreement indicates an independence of the fragmentation process on the exact nature of the excitation mechanism [5].

For ion–fullerene collisions in the kilo electron volt range the energy transfer mechanisms are different because of the extremely short interaction times between projectile and target. Especially collisions of multiply charged ions with fullerenes have been studied in this energy range [6–10]. It was found that interactions of this kind lead to exceptional distributions of the collision products. Highly charged C_{60}^{r+} clusters are formed in a gentle way [Fig. 1(b) and (c);

* Corresponding author. E-mail: tschlat@kvi.nl

PII S1387-3806(99)00108-6

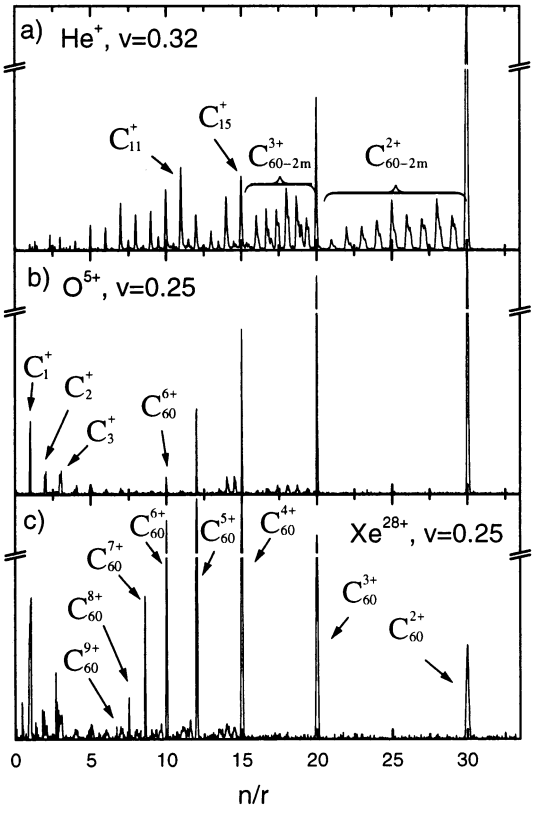

Fig. 1. Mass spectra of the collision products from (a) He^+, (b) O^{5+}, and (c) Xe^{28+} collisions with C_{60}. The projectile velocity in atomic units is given in each plot. In all three plots the break on the intensity axis is at 33% of the strongest peak.

[11,12]] as is obvious from the absence of the comb-like C^{r+}_{60-2m} peaks. For highly charged projectiles, fullerenes with charges up to $r = 9$ are formed [Fig. 1(c), [13]]. In contrast to collisions of singly charged ions with fullerenes, where a broad mass distribution of small fragments is found, for high charge states the distribution of C^+_n peaks at $n = 1$, i.e. very small fragments are formed. Formation of highly charged fullerene ions can be easily explained in terms of gentle electron capture processes occurring at large distances. It is difficult however to find an explanation for the appearance of the small fragments, which are most likely due to violent collision processes.

To shed some light on the above-mentioned physics, we investigate collisions of the simplest multiply charged ions, He^{q+}, with fullerenes over a wide range of collision velocities. In a recent publication [14] we have already shown that inelastic energy losses due to electronic excitation (scaling linear with v) cause multifragmentation and direct ionization whereas direct vibrational excitation (scaling with $1/v$) causes evaporation. The influence of the projectile potential energy on electron capture and fragmentation is studied by comparing experimental data obtained with singly and doubly charged He projectiles.

2. Experiment

2.1. Apparatus

For the present experiment He^{q+} ions are extracted from an electron cyclotron resonance ion source, floated on a potential between 1 and 28 kV. A double gap linear accelerator operated at 13.56 MHz is used to increase the projectile energy up to 105 keV/q. In the collision chamber a fullerene oven is operated at around 700 K. The C_{60} vapour is effused through a nozzle into the collision region where it is crossed by the projectile ion beam.

By means of a static electric field (250 V/cm) all charged collision products are extracted from this region. A reflectron type time-of-flight (TOF) mass spectrometer [15] (resolution $\approx$ 430) is used to determine the charge-to-mass ratio of the fragment ions. The fragments can be detected in coincidence either with an electron emitted during the collision or with charge state resolved projectiles, which serve as the start signal for the TOF measurement. Alternatively, the projectile beam can be chopped and the chopper pulse is used as a start signal. For the present study the latter method is used, in order to collect the collision products independent of the nature of the collision process. Details of the experimental setup can be found in [16].

2.2. He^+ results

Typical n/r spectra of the products from He^+ collisions with C_{60} are shown in Fig. 2. Over the whole energy range, fullerene ions up to charge state

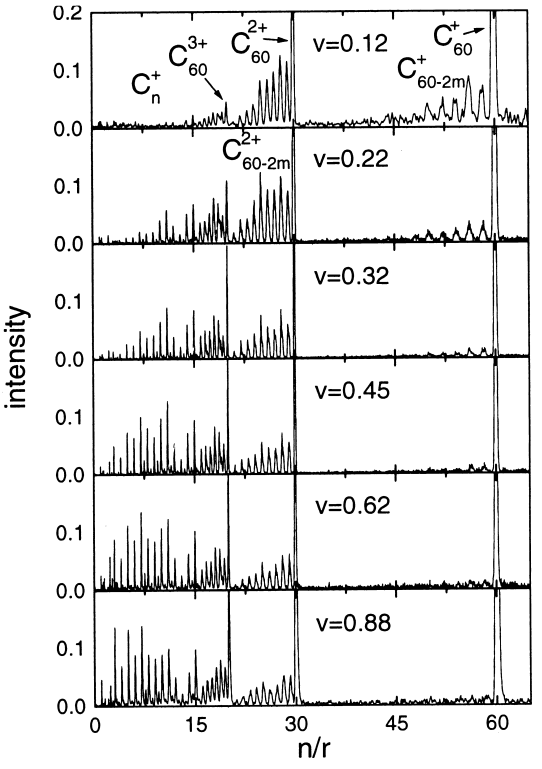

Fig. 2. Mass spectra of C_{60}^{r+} and fragment ions obtained with He^+ projectiles at different collision velocities v (in a.u.). The C_{60}^+ yield is normalized to one and the ordinate ranges from 0 to 0.2.

$r = 3$ are found. We note that for collision energies above 20 keV ($v \approx 0.45$ a.u.) we also observe quadruply charged fullerenes, superimposed on the C_{15}^+ fragment peak. By means of a low extraction field both structures can be clearly separated.

In the spectra, two opposite trends can be observed. (1) The yield of small fragments (C_n^+, $n = 1$–14) increases strongly with collision energy. At low energies, no small fragments are observed while at high energies the small fragment peaks are main features of the spectra. (2) The evaporation peaks (C_{60-2m}^{r+}, $m = 1$–8, $r = 1, 2, 3$) decrease strongly with increasing collision energy.

The relative yield of the small fragments is obtained from the spectra as the ratio of the respective fragment peak integral to the C_{60}^+ peak integral. In Fig. 3 these are shown for $n \leq 14$. At low projectile velocities ($v \leq 0.3$ a.u.) we actually observe small

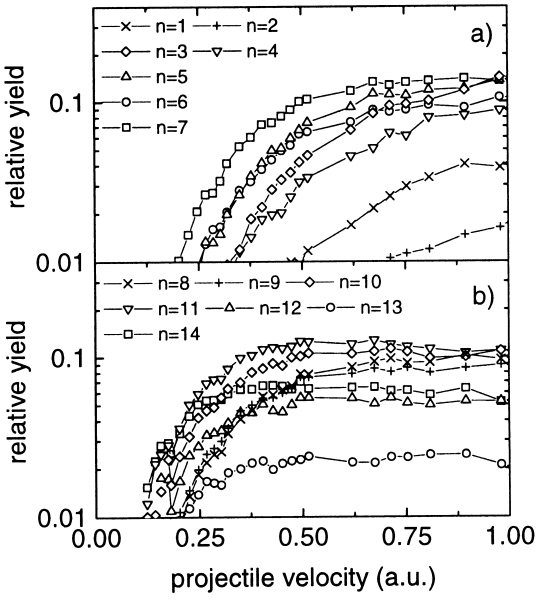

Fig. 3. Relative yields of the small fragments (n = 1–14) with respect to the C_{60}^+ yield for collisions with He^+ projectiles.

amounts of larger fragments up to $n = 19$, but they are partly overlapping with the C_{60-2m}^{3+} structure. All 14 fragment yields increase with the projectile velocity and vanish below a certain threshold velocity.

If we define this appearence threshold at a relative intensity of 1% of the C_{60}^+ yield, no fragments appear below $v = 0.12$ a.u.. It is obvious, that the appearance velocity roughly decreases with increasing cluster size n.

For an easy comparison to the simulation data presented in the next section, relative cross sections for fragmentation σ_f, evaporation $\sigma_{e,1}$ and ionization $\sigma_{i,r}$ have to be defined as

$$\sigma_f = \frac{\sum_{n=1}^{14} \int C_n^+}{\int C_{60}^+ + \sum_{n=1}^{14} \int C_n^+} \quad (1)$$

$$\sigma_{e,1} = \frac{\sum_{m=1}^{9} \int C_{60-2m}^+}{\int C_{60}^+ + \sum_{m=1}^{9} \int C_{60-2m}^+} \quad (2)$$

$$\sigma_{i,r} = \frac{\int C_{60}^{r+}}{\int C_{60}^{+} + \int C_{60}^{r+}}, \quad r = 2, 3 \tag{3}$$

For the relative cross section for evaporation from C_{60}^{2+} a different definition is used:

$$\sigma_{e,2} = \frac{\sum_{m=1}^{9} \int C_{60-2m}^{2+}}{\int C_{60}^{2+} + \sum_{m=1}^{9} \int C_{60-2m}^{2+}} \tag{4}$$

that is the yield of C_{60}^{2+} is taken as a reference. This is done to obtain an evaporation cross section that is independent of the single ionization cross section. It should be mentioned, that in this analysis fission processes of the type

$$C_{60}^{r+} \rightarrow C_{60-2n}^{(r-1)+} + C_{2n}^{+} \tag{5}$$

are neglected. Scheier et al. [17] have recently shown that these processes are unlikely for $r \leq 3$. The results for the fragmentation and evaporation cross section can be found in Fig. 4(a); the ionization cross sections are shown in Fig. 4(b). As can be seen from Fig. 4, multifragmentation and ionization increase with velocity, whereas the evaporation cross section decreases strongly with v. Furthermore, the evaporation cross sections $\sigma_{e,r}$ follow the same slopes with an offset of 0.45 for $r = 2$ with respect to $r = 1$, indicating that the ionization just causes an offset of the evaporation yield.

2.3. He^{2+} results

As compared to He^{+}, collisions of doubly charged He ions with C_{60} lead to substantially different n/r spectra. From Fig. 5 it can be seen, that over the whole energy range C_{60}^{4+} is observed and similar to the He^{+} case, low extraction voltages allow identification of a higher charged fullerene, namely C_{60}^{5+}.

No evaporation from C_{60}^{+} is observed and also the evaporation from C_{60}^{2+} is strongly suppressed as compared to the He^{+} results depicted in Fig. 2. Similar to the He^{+} results, an increase of fragmentation and ionization with v can be found. Analogue to the

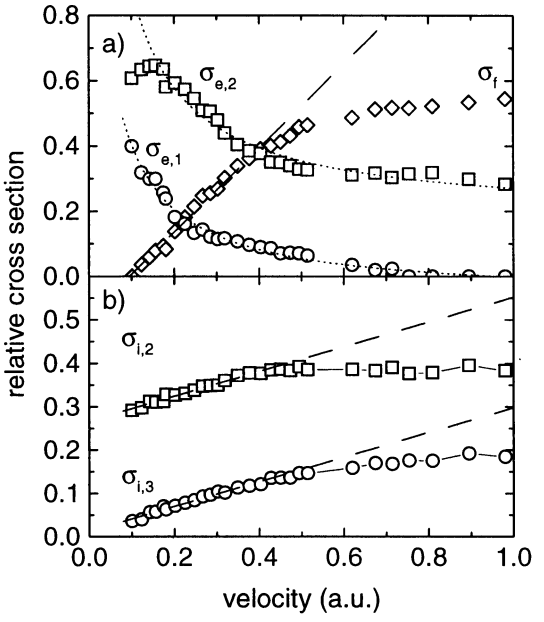

Fig. 4. Relative cross sections for (a) evaporation σ_e and multifragmentation σ_f as well as (b) ionization σ_i of C_{60} in collisions with He^{+}. Note that the evaporation cross section $\sigma_{e,2}$ is calculated with respect to the C_{60}^{2+} yield. The dashed lines are linear fits to the experimental data, the dotted lines in (a) are $(1/v)$ $(\sigma_{e,1})$ and $1/v$ + const $(\sigma_{e,2})$ fits, respectively.

procedure used to evaluate the He^{+} results, we first show the relative yields of small fragments (Fig. 6). Because of the strong C_{60-2m}^{4+} contribution overlapping with the fragment peaks C_{13}^{+} and C_{14}^{+} we only plot the C_n^{+} yields for $n = 1$–12. The slopes of the yields resemble the ones for singly charged projectiles (Fig. 3) but the curves are shifted to lower projectile velocities. The appearance velocities decrease.

Relative cross sections for evaporation, fragmentation, and ionization are defined in the same way as for He^{+}. As mentioned previously, for He^{2+} projectiles no evaporation from C_{60}^{+} is observed. On the other hand, large amounts of C_{60}^{3+} are formed, allowing a quantitative evaluation of the respective evaporation peaks. Fig. 7(a) therefore shows evaporation cross sections for C_{60}^{2+} and C_{60}^{3+} $(\sigma_{e,2}, \sigma_{e,3})$ as well as the fragmentation cross section (σ_f). The trends observed are quite similar to those found for He^{+}: The evaporation decreases strongly with increasing v whereas the fragmentation cross section is increasing.

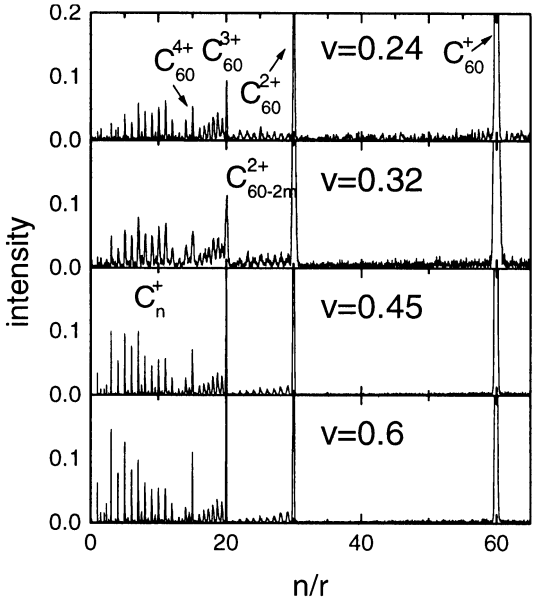

Fig. 5. Mass spectra of the collision products from He^{2+}–C_{60} collisions at different projectile energies.

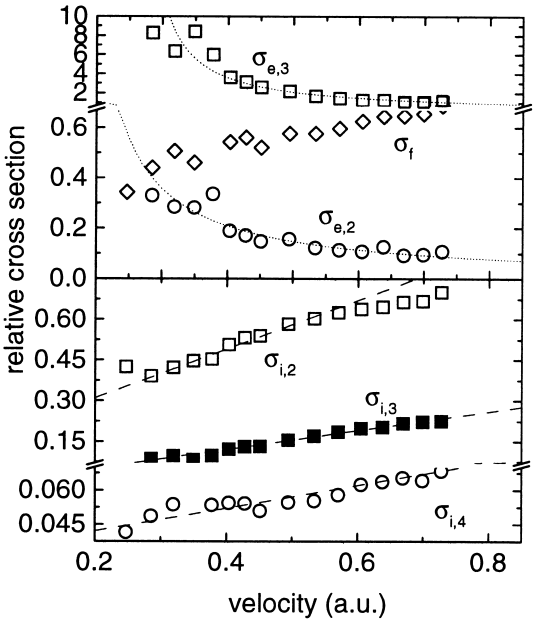

Fig. 7. Relative cross sections for (a) evaporation σ_e and multifragmentation σ_f as well as (b) ionization σ_i of C_{60} in collisions with He^{2+}. Note, that the evaporation cross sections $\sigma_{e,r}$ are calculated in relation to the respective C_{60}^{r+} yields. The dashed lines are linear fits to the experimental data, the dotted lines are $1/v$ fits.

$\sigma_{e,2}$ and $\sigma_{e,3}$ exhibit similar slopes but differ quantitatively from each other by roughly one order of magnitude. (It has to be kept in mind, that these values are relative to the total yield of ions in the respective charge state, the yields with respect to C_{60}^+ are comparable.) Ionization cross sections are displayed in Fig. 7(b). $\sigma_{i,2}$, $\sigma_{i,3}$, and $\sigma_{i,4}$ increase with v. It has to be mentioned however, that in contrast to the He^+ case, C_{60}^{2+} can now also be formed via double electron capture and not only via direct ionization.

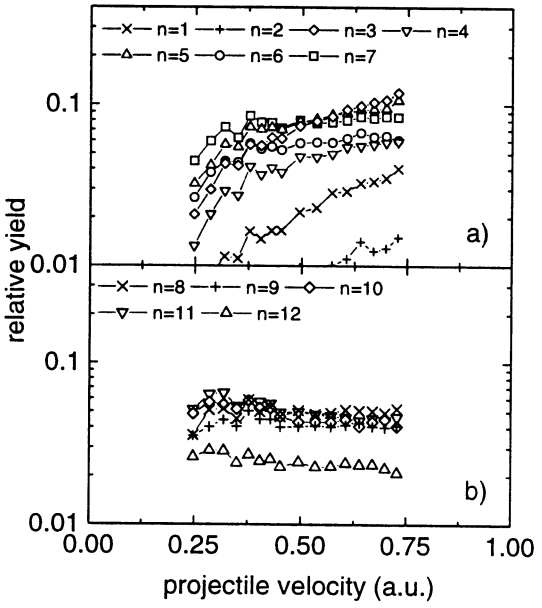

Fig. 6. Relative yields of for the small fragments (n = 1–12) with respect to the C_{60}^+ yield.

3. Simulation

3.1. Trajectory calculations

Molecular dynamics simulations are widely used to model dynamical processes in microscopic systems. For fragmentation dynamics of clusters induced by kiloelectron volt atom or ion impact, the determining stage is the phase where projectile and target interact. In particular, the precise path of the projectile

through the cluster is of importance. To this end we solve Newton's equations numerically along the trajectory of the projectile for the whole collision system. For each launched projectile, the fullerene target orientation is randomly chosen and the internal temperature is set to zero. The projectile starts at (x, y, $-z$) and moves in z direction with a velocity between 0.1 and 1 a.u. x and y are randomly selected and have to fulfill the criterion $x^2 + y^2 \leq R_1^2$ where R_1 is the radius at which the first electron is captured (events where the C_{60} is not ionized do not lead to a signal in our experiment). Using the classical overbarrier model (COM) R_1 is estimated to be 11 and 14 a.u. for He^+ and He^{2+} projectiles, respectively. Each integration step now requires the calculation of the forces acting on the 61 atoms of the system. To obtain realistic results it is crucial to use a C–C potential that is capable of reproducing fullerene properties as well as properties of the various possible fragment clusters. It has been shown that the Brenner-I potential [18] satisfies these requirements for He–fullerene collisions [19]. It has the form

$$V^{\mathrm{C-C}} = \frac{1}{2}\sum_i \sum_{i \neq j} [V_R(r_{ij}) - B_{ij}V_A(r_{ij})] \tag{6}$$

with attractive and repulsive two-body interactions V_A and V_R and r_{ij} being the distance between atoms i and j. For $B_{ij} = 1$ the potential $V^{\mathrm{C-C}}$ has the structure of a Morse potential. B_{ij} is the so-called bond order term containing the sum of three-body interactions. Essentially this term depends on the angles between bonds as well as their lengths.

The interaction of noble-gas atoms with atoms of other species can usually be well described by means of a screened Coulomb potential. We have chosen the screening function of Molière [20] with the screening length adjusted by Ehlich et al. to experimental threshold energies for endohedral complex formation in He–C_{60} collisions [19].

The procedure we used to solve the set of coupled differential equations numerically is the Verlet algorithm [21], a predictor–corrector method. The time steps Δt are of the order of 10^{-16}–10^{-18} s.

3.2. Inelastic energy loss

The described simulation scheme is an appropriate model for the adiabatic part of the He^{q+}–C_{60} interaction. However it is known that for kiloelectron volt collisions of atoms and Na_n^+ clusters electronic excitations of the cluster are becoming important [22]. Recently, Larsson *et al.* [23] found evidence for inelastic energy losses due to electronic excitation in collisions of kiloelectron volt noble gas ions colliding with fullerenes. Estimations based on the Firsov formula [24] are in qualitative agreement but do not take into account the influence of the projectile trajectory through the fullerene.

Because of the large number of delocalized valence electrons the electronic structure of C_{60} has similar properties as the one of a metal and can be well described as an electron gas. We adopt the term of the stopping power S often used in ion–solid collisions, to describe inelastic energy loss of the projectile due to electronic excitations of the target. In the velocity range under study, electronic stopping of ions traveling through an electron gas is due to long range coupling with electron–hole pairs [25] and scales linear with the velocity. The stopping power is defined as

$$S = \frac{dE}{dx} = -\gamma(r_s)v \tag{7}$$

where dE is the energy loss per trajectory section dx [26,27]. The friction coefficient γ is a functional of the density parameter $r_s(R) = [\frac{4}{3}\pi n_0(R)]^{-1/3}$ with the local electron density $n_0(R)$. The valence electron density $n_0(R)$ for the C_{60} is assumed to be a spherically symmetric jellium shell as in [28] with R being the distance from the fullerene center.

The inelastic energy loss due to electronic excitation per simulation time step Δt can now be written as

$$\Delta E = -\gamma(r_s)v\Delta R = -\gamma(r_s)v^2\Delta t \tag{8}$$

The friction term gamma as a function of the density parameter has been calculated by Puska and Nieminen for different values of r_s [29] and can be interpolated by the exponential $\gamma(r_s) = (0.755)\exp$

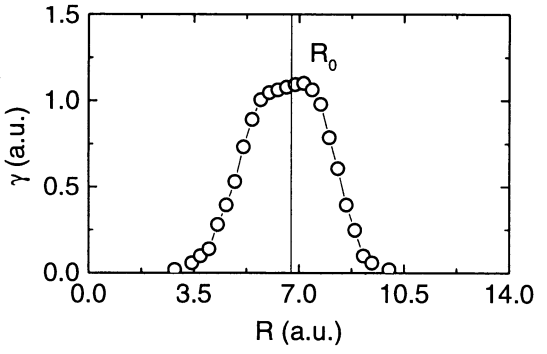

Fig. 8. Friction coefficient γ as a function of the distance from the fullerene center R [28,29]. R_0 indicates the geometric radius of the C_{60}, the asymmetry with respect to R_0 is due to the asymmetric electron density.

([$-(r_s - 1.5)/0.88$]) (unless otherwise stated, here and in the following all values are given in atomic units). Fig. 8 displays γ (R) obtained in this way.

3.3. Results

Statistically relevant results are usually obtained for a set of at least 1000 trajectories. The most interesting calculated quantity for a comparison to our experiments is the kinetic energy transferred from the projectile to the target during the collision process, i.e. the vibrational excitation of the fullerene or the projectile energy loss. In Fig. 9(a) these losses are plotted versus the impact parameter b for collisions of He ($v = 0.27$ a.u.) with C_{60}. Inelastic energy losses are neglected, thus the energy loss is purely elastic. Each point represents one trajectory [note that the point density inherently contains a $2\pi b$ dependence due to the random start coordinates (x, y), $x^2 + y^2 \leq R_1^2$]. By far the highest losses can occur for values of b around 6.5 a.u., the geometric radius of the C_{60}. In this region the projectile experiences the highest density per square centimeter of C atoms. Even in this region, also collisions with negligible energy loss are possible. For more central collisions the average loss is getting smaller just as for glancing collisions with $b > 6.5$ a.u.

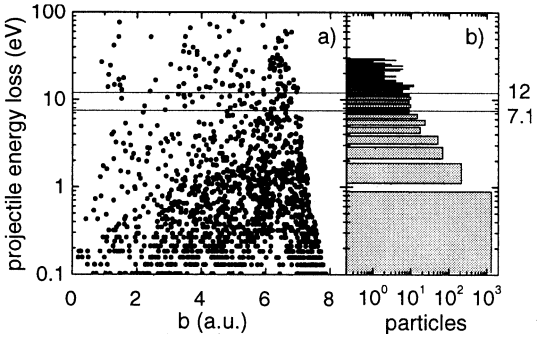

Fig. 9. Simulated projectile energy loss for collisions of He ($v = 0.27$ a.u.) with C_{60} (2000 events). Inelastic energy losses are switched off. (a) Single events as a function of the impact parameter b; (b) histogram with 1 eV bins. Indicated are the theoretically and experimentally obtained thresholds for evaporation (12 and 7.1 eV, respectively).

We obtain the projectile energy loss spectrum by binning the single event losses into 1 eV bins. The resulting spectrum is shown in Fig. 9(b). Obviously, the majority of collisions leads to an energy loss of only a few electron volts. It is known from theoretical [30] as well as experimental studies [31], that the fragmentation threshold for C_{60}, i.e. the internal energy above where evaporation processes are possible, is 12 eV (theory), respectively, 7.1 eV (experiment). These values are indicated in Fig. 9.

Similar to Eq. (2) the absolute cross section for evaporative fragmentation can now be defined as

$$\sigma_e = \frac{Y_{E \geq E_{\text{threshold}}}}{Y_{\text{total}}} \tag{9}$$

i.e. the ratio between events with energy loss above threshold, leading to evaporation, and the total number of events. In Fig. 10, σ_e obtained with the two threshold values is plotted as a function of the projectile velocity. Both curves are proportional to $1/v$ indicating a linear dependence between kinetic energy loss and projectile–target interaction time. It should be noted, that a recent experimental study of Laskin *et al.* [32] revealed evidence for a threshold value close to 10 eV, approaching the theoretical value. Furthermore, the above mentioned threshold energy evaporation can occur over a time scale of up to several microseconds. Therefore the threshold energy for prompt evaporation (within less than 1 μs) is probably higher, according to Laskin *et al.* as high as

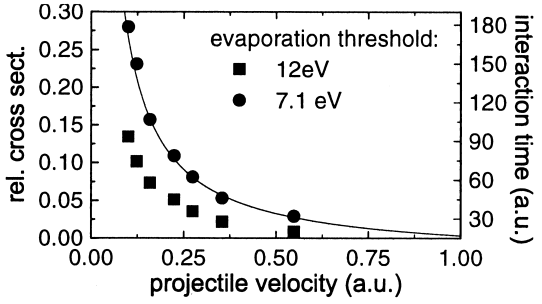

Fig. 10. Simulated cross sections for evaporation induced by direct vibrational excitation (σ_e) obtained for the two different threshold values (see text). Inelastic energy losses are switched off. The solid line is a $1/v$ fit, on the right axis the respective interaction time can be found.

around 40 eV. However, the qualitative velocity dependence of the cross section should not be affected by both facts, even though the absolute values for σ_e could be much lower than in Fig. 10. The latter underlines the important role of electronic stopping even more.

If the electronic stopping is taken into account, the projectile energy loss distribution changes dramatically. The results for He collisions with C_{60} (v = 0.27 a.u.) are shown in Fig. 11. It is obvious, that the scatter of the loss due to direct vibrational excitation [see Fig. 9(a)] is superimposed on the inelastic loss (due to electronic excitation) as a function of b. For central collisions ($b \approx 0$) the projectile passes the

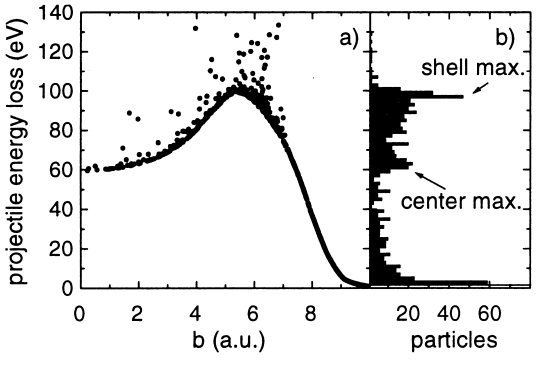

Fig. 11. Simulated projectile energy loss for collisions of He (v = 0.27 a.u.) with C_{60} (1000 events). Inelastic energy losses are switched on. (a) Single events as a function of the impact parameter b; (b) histogram with 2 eV bins.

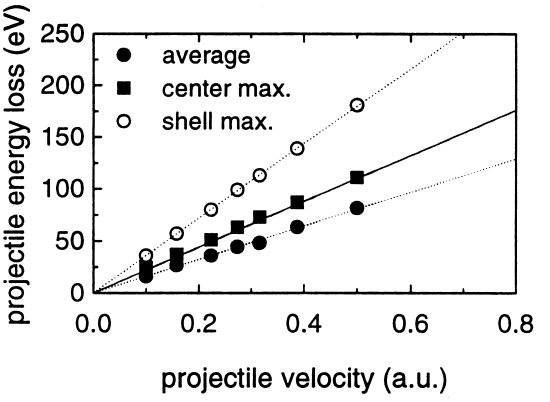

Fig. 12. Simulated projectile energy losses as a function of the velocity. Inelastic energy losses are switched on. The symbols indicate the average energy loss (full circles) as well as the losses for central and shell collisions (full squares and open circles, respectively), as indicated in Fig. 11(b). The dotted lines are linear fits and the solid line follows Eq. (10).

fullerene shell twice and an energy loss of ≈60 eV is found (center maximum). With increasing b, the electronic stopping contribution to the total loss increases to more than 100 eV, due to the long section of the trajectory passing through high electron density regions of the fullerene (shell maximum). Impact parameters larger than the geometrical fullerene radius lead to glancing collisions and small electronically induced inelastic energy loss values. The projectile energy loss spectrum is completely different from what is obtained without electronic stopping. The average energy loss is of the order of 50 eV and the distribution consists of three maxima due to the three different interaction regimes mentioned above [Fig. 11(b)].

For collisions with $b \approx 0$, the inelastic loss can be calculated analytically.

$$\Delta E = \int_{-\infty}^{\infty} -\gamma[r_s(R)]v\,dx$$

$$\approx 2v \int_{0}^{\infty} -\gamma[r_s(R)]\,dx \approx 8.1v \qquad (10)$$

This is in good agreement with the simulated projectile energy losses for $b \approx 0$ (see Fig. 12, for central

collisions). Also the average projectile energy loss obtained from the simulations including electronic stopping scales linearly with v and the same holds for the loss observed for collisions with the fullerene shell.

4. Discussion

4.1. He^+

In Sec. 3 it was pointed out that in the system under study two excitation mechanisms are predicted to be important, namely direct vibrational as well as electronic excitation.

In a recent publication Campbell et al. [5] have investigated collisions of C_{60}^+ with Xe and Ar atoms at center-of-mass collision energies between 16 and 250 eV theoretically. They predict a phase transition from evaporation to multifragmentation with increasing internal energy. The excitation mechanism itself apparently plays no role for the fragmentation dynamics in this collision energy range. Their calculated fragmentation patterns are in good agreement with experimental results from collision studies [4] as well as from multiphoton ionization experiments [33]. Our results however indicate that this independence of the fragmentation pattern from the excitation process is lifted at kiloelectron volt collision energies, at least for light projectiles such as He. (Heavy projectiles such as Ar cannot pass the fullerene cage without destroying it even at high relative velocities. Studies regarding the transition from light to heavy projectiles are in progress.)

According to the simulation, direct vibrational excitation of the fullerene leads to relatively small internal energies which eventually exceed the evaporation threshold (Fig. 9). We call this mechanism *e*vaporation induced by *v*ibrational *e*xcitation (EVE) [14]. The $1/v$ scaling of the evaporation cross section σ_e (v being the projectile energy) can be directly recognized in the experimental data for He^+ collisions with C_{60} (Fig. 4). $\sigma_{e,1}$ as well as $\sigma_{e,2}$ follow an $1/v$ scaling, the only difference being an offset of $\approx$0.25 to higher values for the $\sigma_{e,2}$ data. Under the assumption, that the evaporation from C_{60}^+ is indeed due to direct vibrational excitation only, the offset can be explained straightforward: For an additional electron removal from the C_{60}^+ the excitation energy has to exceed the respective ionization potential (11.5 eV [34,35]). The ionization is always accompanied by an average vibrational excitation which in turn leads to evaporation. The fact, that $\sigma_{e,2}$ still shows the $1/v$ scaling then implies an invariance of this ionization induced evaporation with the velocity v. The average vibrational excitation accompanying the ionization is constant.

σ_e obtained from the simulation is roughly a factor of 2 smaller than the experimentally observed $\sigma_{e,1}$. The reason is the presence of fragmentation processes which arise from electronic excitations of the fullerene.

These electronic excitations are mainly due to the previously mentioned electronic stopping of the projectile moving through the electron gas of the fullerene. It has been shown in Sec. 3.3 that such a mechanism should lead to an energy deposition in the fullerene, which increases linearly with projectile velocity (Fig. 12). In the experimental data for the collisions of He^+ with C_{60} a linear dependence of v is found for the multifragmentation cross section σ_f [Fig. 4(a)]. We therefore call the underlying mechanism *f*ragmentation due to *e*lectronic *e*xcitation (FEE). Note, that our main argument supporting the EVE model is the scaling of σ_e. The linear increase of the electronic stopping (and therefore of the total excitation energy) with v might also cause a drop in the evaporation probability if the EVE and FEE processes were not separated. In the latter case the increasing cross section for multifragmentation would inherently induce a decrease of evaporation.

The appearance velocities as a function of the carbon cluster size n are plotted in Fig. 13(a). As mentioned before, the appearance threshold is defined as 1% of the C_{60}^+ yield. (Slightly different thresholds do not considerably change the slope of the curve but rather shift it to higher or lower velocities. We have chosen the 1% limit since below no clear separation between peak and background was possible for some of the smallest clusters.)

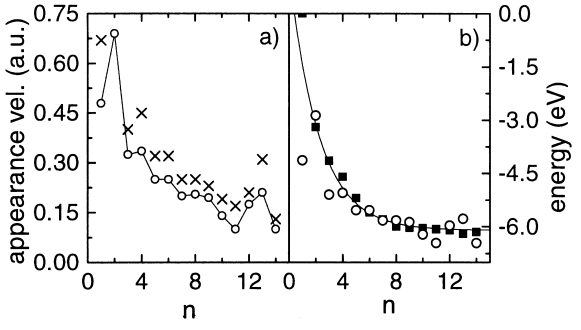

Fig. 13. (a) Appearance velocities obtained from Fig. 3 (threshold is 1% of the C_{60}^+ yield, results for a 2% threshold are plotted as crosses). (b) Binding energies per carbon atom as obtained from the appearance velocities (open circles) and from theory (solid squares, [19]). The solid line is an exponential fit to the theoretical values. All quantities are plotted as a function of the cluster size n.

The C_{60} (binding energy per atom $E_b^{C_{60}} \approx 7.04$ eV) can break into C_n clusters (binding energy $E_b^{C_n}$) when its excitation energy exceeds $E_b^{C_{60}} - E_b^{C_n}$. Note, that this is the worst case scenario, assuming a breakup into equally sized fragments. A fragment cluster C_n can already appear at lower excitation energies, then accompanied by larger fragments. Also the threshold for the appearance velocities is defined arbitrarily. The following discussion is therefore a qualitative one. The maximum excitation energy at a given v_{app} is deposited into the fullerene after a shell collision. From the simulation results in Fig. 12 we can obtain this energy (note, that in Fig. 12 the total energy is plotted and here we use the energy per carbon atom). Subtracting this energy from $E_b^{C_{60}}$ gives the binding energy $E_b^{C_n}$ of the weakest bound fragment cluster that can be formed at v_{app} [Fig. 13(b)].

The appearance velocities (and the obtained binding energies) show some oscillation with n reflecting the magic numbers 11 and 15 (Fig. 13 just ranges to $n = 14$, from the raw data the appearance velocity for $n = 15$ can be estimated to be smaller than for $n = 14$). These clusters are found as prominent peaks in most fragmentation studies [36–38]. Their importance might be due to the special stability of $4n + 2$ carbon rings which lost a C_3 fragment [39]. The plotted binding energies of Ehlich et al. [19] have been obtained using an analytical potential, i.e. effects of the electronic structure are averaged out. We therefore use the exponential fit to the data (dotted line in Fig. 13) to be compared to the energies obtained from the appearance velocities.

Down to $n = 2$, the slopes of appearance velocities and the binding energies coincide, demonstrating again the linear dependence of multifragmentation and projectile velocity. For small n, the theoretical values systematically exceed the results obtained from the appearance velocities. This is due to the fact, that we made the assumption that the fullerene roughly breaks into fragments of size n. For smaller n, this is certainly not true anymore.

A linear scaling with v is also found for the ionization cross sections $\sigma_{i,r}$ [Fig. 4(b)], indicating that direct ionization is also induced by electronic stopping and thus related to FEE. The cross sections for $r = 2$ and $r = 3$ show a parallel behaviour. All FEE related quantities show a strong deviation from the linear scaling for velocities larger than 0.6 a.u. One possible explanation is that the appearance velocities for the smallest clusters have already been passed and additional excitation might go into kinetic energy of the fragments and not into bond breaking anymore. This is supported by the slopes of the relative yields of the small fragments in Fig. 3. From their respective appearance velocities on the yields always show a strong increase until a saturation value is reached. Hence, for sufficiently high velocities the system apparently prefers a certain statistical distribution of fragment cluster sizes.

Additional processes such as plasmon excitation might also become important for high projectile velocities, thereby affecting the fragmentation dynamics.

Our findings support a coexistence of FEE and EVE over the whole collision velocity range under study which is in contrast to what is found for sub-kiloelectron volt energies. As mentioned previously Campbell *et al*. [5] found the fragmentation pattern to be independent of the excitation mechanism. According to their calculations, a phase transition between evaporation and multifragmentation occurs for fullerene excitation energies between 80 and 225 eV and the appearance energies for the small fragments are almost constant. According to our

simulation, a maximum excitation energy (shell maximum) of 80 eV is only reached for He^+ velocities higher than 0.25 a.u. (see Fig. 12) where the experiment shows that the evaporation cross section already dropped to less than 50% of its original value, i.e. most of the "transition" has already happened. Also the fact, that in our case the appearance velocities and thus the appearance energies depend strongly on the cluster size n is in contrast to the findings at low collision energies.

4.2. He^{2+}

The main difference when going from He^+ to He^{2+} projectiles is the potential energy which increases from 24.6 eV to 24.6 + 54.4 = 79 eV. Where does this additional energy go? It is obvious from the relative yields of small fragments C_n^+ that the slopes obtained with He^+ and He^{2+} are quite similar. Even though we cannot obtain appearance velocities for $n > 3$ from Fig. 6 it can be seen, that for all cluster sizes n the curves are shifted to lower velocities with respect to the He^+ results from Fig. 3.

In particular, for the smallest clusters (n = 1–3) v_{app} is lowered by $v_{app}^{He^+} - v_{app}^{He^{2+}} = 0.47 - 0.31 = 0.16$ a.u. (n = 1), $0.71 - 0.6 = 0.11$ a.u. (n = 2) and $0.34 - 0.235 = 0.105$ a.u. (n = 3). Therefore also the maximum energy loss (shell maximum, open circles in Fig. 12) at the appearance velocity decreases when going from He^+ to He^{2+}. For C clusters with n = 1–3 the values are

$$\Delta E^{He^+} - \Delta E^{He^{2+}} = 112 - 57 = 55 \text{ eV}(n = 1) \quad (11)$$

$$\Delta E^{He^+} - \Delta E^{He^{2+}} = 217 - 179 = 38 \text{ eV}(n = 2) \quad (12)$$

$$\Delta E^{He^+} - \Delta E^{He^{2+}} = 85 - 60 = 25 \text{ eV}(n = 3) \quad (13)$$

Clearly the lower excitation energy can be balanced by the additional potential energy of the doubly charged projectile (54.4 eV).

The relative cross sections for evaporation, fragmentation, and ionization in Fig. 7 also show similarities to the He^+ results. $\sigma_{e,2}$ and $\sigma_{e,3}$ show the usual $1/v$ scaling of the EVE process whereas $\sigma_{i,2}$, $\sigma_{i,3}$, and $\sigma_{i,4}$ show a linear scaling with v, as expected for FEE related quantities. The multifragmentation cross section σ_f increases with v.

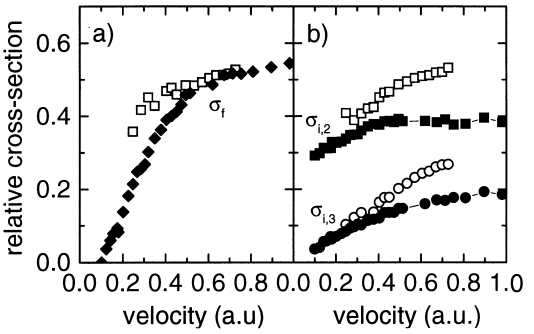

Fig. 14. Relative cross sections for multifragmentation (σ_f, a) and ionization ($\sigma_{i,r}$, b) of C_{60} in collisions with He^{q+}. Open symbols: He^{2+}; full symbols: He^+. The He^{2+} results are scaled to account for the different one electron capture cross sections (see text).

To compare the relative cross sections obtained with singly and doubly charged He it is essential to put the respective quantities on equal scales. According to the COM the capture radii for production of C_{60}^+ are roughly 11 and 14 a.u. for He^+ and He^{2+} projectiles, respectively. The C_{60}^+ yield obtained with He^{2+} therefore has to be weighted with the ratio of the one-electron capture cross sections for He^+ and He^{2+} projectiles, i.e. with $11^2/14^2$.

Fig. 14 displays the multifragmentation cross sections σ_f and the ionization cross sections $\sigma_{i,r}$ as a function of the projectile velocity.

Two opposite trends can be observed for multifragmentation and ionization, respectively: The σ_f values for He^{2+} exceed those for He^+ at low v [Fig. 14(a)]. With increasing velocity the difference vanishes until comparable results are found. The ionization cross sections behave the other way round and differ for high v, whereas for low v comparable values are measured. This phenomenon can be explained in the same way as the suppressed potential electron emission of slow multicharged fullerenes on metals, recently observed by Winter et al. [40]: If the collision time is long enough the intermediate $(He–C_{60})^{2+}$ complex has time to relax and the additional potential

energy is efficiently converted into vibrational excitation leading to fragmentation of the fullerene. For shorter collision times this coupling is suppressed and direct emission of electrons is taking over. The transition between fragmentation and ionization takes place at $v = 0.3–0.5$ a.u. These velocities correspond to collision times between 1.4 and 2.2 fs when assuming a collision length of 28 a.u. (two times the first capture radius of He^{2+}). The drawback of this explanation is, that these times are 2–3 orders of magnitude shorter than the typical coupling times between electronic and vibrational excitation in molecules: The conversion would therefore require a different mechanism.

5. Conclusion

The influence of projectile velocity and potential energy of He^{q+} projectiles on fullerene ionization and fragmentation has been studied. Two different processes could be identified to be active in such collisions. Evaporation is induced by direct vibrational excitation of the fullerene (EVE) whereas multifragmentation is due to electronic excitations (FEE), i.e. electronic stopping. The excess potential energy of He^{2+} couples to the electronic excitation of the collision complex and amplifies the FEE related channels multifragmentation and ionization. For high velocities mainly the ionization cross section increases and for low velocities the additional energy leaves its fingerprint as increased small fragment yields.

Acknowledgements

This project has been part of the research program of the “Stichting voor Fundamenteel Onderzoek der Materie” (FOM). One of the authors (T.S.) acknowledges financial support from the EC within the Marie Curie Fellowship program, contract no. ERBFMBICT961704.

References

[1] B. Dünser, M. Lezius, P. Scheier, H. Deutsch, T.D. Märk, Phys. Rev. Lett. 74 (1995) 3364.
[2] H. Hohmann, C. Callegari, S. Furrer, D. Grosenick, E.E.B. Campbell, I.V. Hertel, Phys. Rev. Lett. 73 (1994) 1919.
[3] D.C. Lorents, Comments At. Mol. Phys. 33 (1997) 125.
[4] R. Ehlich, M. Westerburg, E.E.B. Campbell, J. Chem. Phys. 104 (1996) 1900.
[5] E.E.B. Campbell, T. Raz, R.D. Levine, Chem. Phys. Lett. 253 (1996) 261.
[6] U. Thumm, A. Barany, H. Cederquist, L. Hägg, C.J. Setterlind, Phys. Rev. A 56 (1997) 4799.
[7] H. Shen, P. Hvelplund, D.C. Lorents, D. Mathur, Chem. Phys. Lett. 264 (1997) 508.
[8] S. Martin, L. Chen, A. Denis, S. Desesquelles, Phys. Rev. A57 (1998) 4518.
[9] A. Reinköster, U. Werner, H.O. Lutz, Europhys. Lett. 43 (1998) 653.
[10] B. Walch, U. Thumm, M. Stöckli, C.L. Cocke, S. Klawikowski, Phys. Rev. A 58 (1998) 1261.
[11] B. Walch, C.L. Cocke, R. Voelpel, E. Salzborn, Phys. Rev. Lett. 72 (1994) 1439.
[12] T. Schlathölter, R. Hoekstra, R. Morgenstern, J. Phys. B.: At. Mol. Opt. Phys. 31 (1998) 1321.
[13] J. Jin, H. Khemliche, M.H. Prior, Z. Xie, Phys. Rev. A 53 (1996) 615.
[14] T. Schlathölter, O. Hadjar, R. Hoekstra, R. Morgenstern, Phys. Rev. Lett. 82 (1999) 73.
[15] B.A. Mamyrin, V.I. Karatev, A.A. Shmikk, V.A. Zagulin, Sov. Phys. JETP 37 (1973) 45.
[16] H.O. Folkerts, F.W. Bliek, M.C. de Jong, R. Hoekstra, R. Morgenstern, J. Phys. B: At. Mol. Opt. Phys. 30 (1997) 5833.
[17] P. Scheier, B. Dünser, T.D. Märk, Phys. Rev. Lett. 74 (1995) 3368.
[18] D.W. Brenner, Phys. Rev. B 42 (1990) 9458.
[19] R. Ehlich, E.E.B. Campbell, O. Knospe, R. Schmidt, Z. Phys. D 28 (1993) 153.
[20] G. Molière, Z. Naturforsch. A2 (1947) 133.
[21] L. Verlet, Phys. Rev. 159 (1967) 98.
[22] J.C. Brenot, H. Dunet, J.A. Fayeton, M. Barat, M. Winter, Phys. Rev. Lett. 77 (1996) 1246.
[23] M.O. Larsson, P. Hvelplund, M.C. Larsen, H. Shen, H. Cederquist, M.T. Schmidt, Int. J. Mass Spectrom. Ion Processes 177 (1998) 51.
[24] E.S. Parilis, Nucl. Instrum. Methods Phys. Res. B 88 (1994) 21.
[25] T.L. Ferrel, P.M. Echenique, R.H. Ritchie, Solid State Comm. 32 (1979) 419.
[26] A. Närmann, R. Monreal, P.M. Echenique, F. Flores, W. Heiland, S. Schubert, Phys. Rev. Lett. 64 (1990) 1601.
[27] A. Närmann, W. Heiland, R. Monreal, F. Flores, P.M. Echenique, Phys. Rev. B 44 (1991) 2003.
[28] M.J. Puska, R.M. Nieminen, Phys. Rev. A 47 (1993) 1181.
[29] M.J. Puska, R.M. Nieminen, Phys. Rev. B 27 (1983) 6121.
[30] W.C. Eckhoff, G.E. Scuseria, Chem. Phys. Lett. 216 (1993) 399.

[31] M. Foltin, M. Lezius, P. Scheier, T.D. Märk, J. Chem. Phys. 98 (1993) 9624.
[32] J. Laskin, B. Hadas, T.D. Märk, C. Lifshitz, Int. J. Mass Spectrom. Ion Processes 177 (1998) L9.
[33] H. Hohmann, R. Ehlich, S. Furrer, O. Kittelmann, J. Ringling, E.E.B. Campbell, Z. Phys. D 33 (1995) 143.
[34] H. Steger, J. Holzapfel, A. Hielscher, W. Kamke, I.V. Hertel, Chem. Phys. Lett. 234 (1995) 455.
[35] S. Matt, O. Echt, R. Wörgötter, V. Grill, P. Scheier, C. Lifshitz, T.D. Märk, Chem. Phys. Lett. 264 (1997) 149.
[36] S. Cheng, H.G. Berry, R.W. Dunford, H. Esbensen, D.S. Gemmell, E.P. Kanter, T. LeBrun, Phys. Rev. A 54 (1996) 3182.
[37] P. Hvelplund, L.H. Andersen, H.K. Haugen, J. Lindhard, D.C. Lorents, R. Malhotra, R. Ruoff, Phys. Rev. Lett. 69 (1992) 1915.
[38] R. Vandenbosch, B.P. Henry, C. Cooper, M.L. Gardel, J.F. Liang, D.I. Will, Phys. Rev. Lett. 81 (1998) 1821.
[39] M.E. Geusic, T.J. McIlrath, M.F. Jarrold, A. Bloomfield, R.R. Freeman, W.L. Brown, J. Chem. Phys. 84 (1986) 2421.
[40] HP. Winter, M. Vana, G. Betz, F. Aumayr, H. Drexel, P. Scheier, T.D. Märk, Phys. Rev. A 56 (1997) 3007.